Available online at www.sciencedirect.com

ScienceDirect

Energy Procedia 148 (2018) 471–478

Energy Procedia

www.elsevier.com/locate/procedia

73rd Conference of the Italian Thermal Machines Engineering Association (ATI 2018), 12-14 September 2018, Pisa, Italy

Heat transfer enhancement induced by the geometry of a LHTES device

F. Fornarelli[a,*], M. Valenzano[a], B. Fortunato[a], S.M. Camporeale[a], M. Torresi[a], P. Oresta[a]

[a]*Dipartimento di Meccanica, Matematica e Managment (DMMM), Politecnico di Bari, via Orabona 4, 70125 Bari, Italy*

Abstract

In the present contribution the authors investigate by means of numerical simulations the thermal performance of two geometries of Latent Heat Thermal Energy Storage (LHTES). The numerical model takes into account the mass, momentum and energy equations for the PCM together with an Entalphy-Porosity model for the phase change and a Bussinesq approximation for the buoyancy force. Indeed in such a system the convective motion within the melted PCM plays an important role, as confirmed by several studies. The scope of the research has been the enhancement of heat transfer performance of LHTES increasing the convection by means of modifications on the shape of the PCM enclosure. In particular, in this study two geometries have been considered to investigate the influence of the convective motion on the overall melting time. The first case consists of two concentric cylinders with the axis aligned with the vertical direction, in order to realize an internal heating of the Phase Change Material (PCM) that is confined between the internal and the external cylinder. It is a well-known "shell-and-tube" configuration, generally adopted in LHTES systems, even in CSP applications. In the second case, the authors propose a simple cylindrical geometry filled with the PCM, with the cylinder axis aligned with the vertical position. Thus, the heated surface corresponds to the external lateral surface of the cylinder. The PCM volume (V) and the net heat transfer surface (A) have been kept constant in the two cases, in order to be able to compare them under the same operative conditions. The tests reveal a sensible difference between the thermal performance of the two proposed solutions. The external heating configuration shows an important enhancement of the convective motion within the PCM that induces a more efficient heat transfer with respect to the standard "shell-and-tube" configuration. The complete melting time of the PCM with external heating is reduced by about 50%.

Keywords: LHTES; PCM; shell-and-tube; convection; CFD

*Corresponding author. Tel.: + 39 080 5963491; fax: + 39 080 5963411
E-mail address: francesco.fornarelli@poliba.it

10.1016/j.egypro.2018.08.122

1. Introduction

Nowadays, the integration of several renewable and conventional energy production systems requires a high flexibility in order to maintain high efficiency of the overall production system [18, 15]. In this scenario, the distributed energy production takes advantage with respect to the concentrated energy systems due to their faster response to the demand change and modularity, in order to include heterogeneous technologies of energy production. Thus, an important component, able to manage the matching between the production systems and the energy demand, is represented by the energy storage. Among the others, in the Concentrated Solar Power plant (CSP) the variation of the solar input during the day could affect negatively the efficiency and, indeed, the availability of such renewable energy source. Therefore, the thermal energy storage has an important role in the improvement of the performance of energy production systems [5, 6]. In particular, according to the working temperatures, phase change materials (PCMs) are chosen in order to improve the performance of the storage in terms of energy density and characteristic time of thermal charging and discharging [17, 1]. In these hypothesis, the heat is stored in PCMs, including both the sensible heat of each phase (i.e. solid and liquid) and the latent heat of the phase change. This kind of device is known as Latent Heat Thermal Energy Storage (LHTES). LHTES performance is influenced by several physical phenomena, including the heat transfer between a Heat Transfer Fluid (HTF) and the PCM, the convective heat transfer in the HTF and in the PCM and the phase change of PCM. In the literature, several works about the energy storage can be found. Different aspects are studied in order to improve the heat exchange of such devices. In particular, the applications can be split according to the natural or forced convection mechanism in the PCM [10], the adding of fins or geometrical shape configuration to enhance the heat transfer, and the operative PCM's melting temperatures. Here, the authors compare the effect of the LHTES geometrical configuration on its charging time. Thus, two geometries are considered: the first considers the classical shell-and-tube configuration, where the HTF flows within the internal duct (tube) that is embraced by an external enclosure (shell) filled by the PCM; the second considers a simple cylindrical enclosure filled by PCM, whereas the HTF surrounds it, wetting the lateral surface of the cylinder. In this preliminary work, the comparison has been made considering the same volume of PCM, that corresponds to the same storable energy, the same external temperature and heat exchange surface area for both the cases under study.

Nomenclature

LHTES	Latent heat thermal energy storage
PCM	Phase change materials
HTF	Heat transfer fluid
CSP	Concentrated solar plant
$\bar{u}$	Fluid velocity
ρ	Density
p	Pressure
g	Gravitational acceleration
$\bar{\bar{\tau}}$	Viscous stress tensor
H	Enthalpy
k	Thermal conductivity
T	Temperature
Λ	Latent heat of melting
c_p	Specific heat
β_l	Liquid fraction
r	Cylinder radius
L	Cylinder height
V	PCM volume
A	Area of heat transfer surface
A_{mush}	Mushy zone constant

2. Numerical setup

The numerical simulations are based on the finite volume discretization approach in order to solve the governing equations of the problem. In particular, the flow field and the heat transfer are modelled according to the Navier-Stokes equations and the energy equation.

$$\nabla \cdot \bar{u} = 0 \tag{1}$$

$$\rho\left(\frac{\partial \bar{u}}{\partial t} + \bar{u}\nabla\bar{u}\right) = -\nabla p + \rho'\bar{g} + \bar{S} + \nabla \cdot \bar{\bar{\tau}} \tag{2}$$

$$\rho\frac{\partial(H)}{\partial t} + \rho\nabla(H\bar{u}) = \nabla(k\nabla T). \tag{3}$$

where $\bar{u}$ is the flow velocity, ρ is the fluid density, $\bar{\bar{\tau}}$ is the viscous stress tensor, μ is the dynamic viscosity, H is the enthalpy, k is the thermal conductivity and T is the temperature.

In the equation 2 two forcing terms appear in the right hand side, specifically the buoyancy term ($\rho'\bar{g}$) and the source term (S). The buoyancy term couples the Navier-Stokes equation with the energy equation in order to model the convective flow within the PCM according to the relation:

$$\rho' = \rho(1 - \alpha\Delta T) \tag{4}$$

where ΔT is the temperature difference with respect to a reference temperature and α is the thermal expansion coefficient. The source term S is introduced to model the behaviour of the PCM during the phase change. According to the *Carman-Kozeny* equation, it reads:

$$S = \frac{(1-\beta_l)^2}{(\beta_l^3 + \epsilon)} A_{mush}\vec{u} \tag{5}$$

in which A_{mush} is the mushy zone constant that is set to 10^5 and β_l is the local liquid fraction linearly related to the melting temperatures as follows:

$$\beta_l = \begin{cases} 0 \quad if \quad T < T_{sol} \\ \frac{T-T_{sol}}{T_{liq}-T_{sol}} \quad if \quad T_{sol} < T < T_{liq} \\ 1 \quad if \quad T > T_{liq} \end{cases} \tag{6}$$

The model here presented is implemented in the commercial CFD software Ansys Fluent according to the enthalpy-porosity approach [13, 14, 2, 19, 20, 16, 4].

The HTF flow is not included in the simulation, however a constant temperature has been fixed on the heated surface. Therefore, the temperature of the hot wall has been kept constant at the same temperature for both the cases under study, $T_w = 523.15K$. Thus, the two geometrical configurations operate under the same boundary conditions.

The study considers two geometries: a shell-and-tube geometry (case 1) where the heated surface corresponds to the internal lateral surface of the inner cylinder and a cylindrical geometry; and a simple cylindrical enclosure filled with the PCM and heated from the external lateral surface of the cylinder (case 2). The geometrical details of the two cases are reported in tab. 1. A schematic of the geometries under study are reported in fig. 1. Even though the geometrical configuration is different, the volume and the heat exchange area has been kept constant. It is worth noting

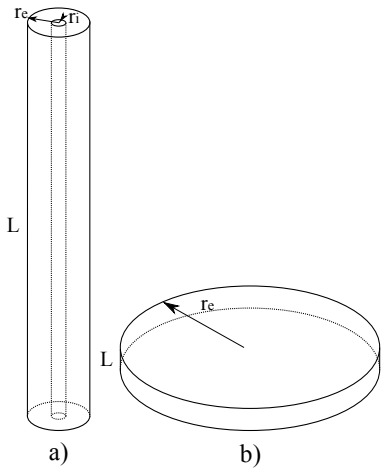

Fig. 1. Schematic of the geometries of the PCM enclosures of the test cases here presented. The PCM volume $V = 1.82 \cdot 10^{-3} m^3$, and the heat transfer surface area $A = 2.51 \cdot 10^{-2} m^2$ are constant for each case. a) internal heating (case 1), b) external heating (case 2)

Table 1. Geometrical details of the test cases

	case 1	case 2
Heating	Internal	External
r_e $[mm]$	35	145
r_i $[mm]$	8	–
L $[mm]$	500	27.6
V/A $[1/m]$	0.0725	0.0725

that the geometry used in case 1 is just one of the possible combination of geometrical parameters (r_e, r_i and L) that satisfy the constrain on the surface area and the volume of the PCM. It has been chosen according to previous studies of the author based on a comparison of the model with experimental device [6, 7] . Then, the second case has a big radius and a small height due to the constrain on volume and heat exchange area. In fig. 2 two possible applications are proposed in order to implement the two geometries in two heat storage modules. The case 1 corresponds to the standard shell-and-tube configuration, where the HTF flows within the tubes within the PCM (see fig. 2b). . Whereas, in case 2 the HTF has to flow around the lateral surface of the cylinders filled with the PCM that can be stacked up. For instance, a cross-flow configuration is proposed (see fig. 2b). The proposed application of case 2 could has the advantage to simplify the HTF flow with respect to the shell-and-tube geometry (case 1) and the PCM modules distribution could be optimized according to in-line or staggered configuration as in tube bundle heat exchangers [8, 9]. The number of grid cells have been chosen according to a detailed grid independence study. For case 1 and 2, 428400 and 444400 grid cells have been considered, respectively, with an axisymmetric 2D non uniform Cartesian mesh.

The physical properties of the PCM are reported in tab. 2, and they correspond to the typical characteristics of a binary mixture of melted salts ($NaNO_3 60\%wt - KNO_3 40\%wt$).

3. Results

The analysis has been made considering the initial temperature below the solidus temperature of the PCM ($T_{in} = 423K$) in the whole domain. The heated wall temperature has been kept constant to $T_w = 523K$ and the PCM starts to warm up till to the complete melting. As already described in the literature [21, 22, 3, 11, 12], a continuous melting front can be recognized, within the PCM, whose velocity is strictly related to the heating rate. Thus, higher the velocity of the front is, faster the heat rate will be. In case 1, where the hot wall corresponds to the internal radius of the shell geometry the behaviour of the PCM has been reported according to the liquid fraction contours at different time steps

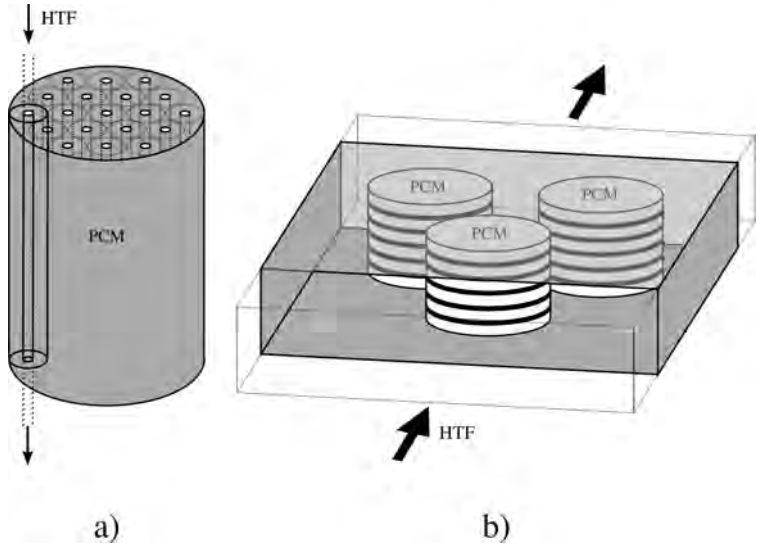

Fig. 2. Schematics of the storage module for the two configurations here studied. a) case 1, shell-and-tube configuration where the HTF flow within the tubes through the heat storage filled with PCM; b) case 2, external heating with a cross flow between the HTF and the cylindrical PCM modules stacked up.

Table 2. Physical properties of the PCM. T is in K.

Properties	Values	
Density	$\rho_{PCM} = 1994$	$\left(\frac{kg}{m^3}\right)$
Thermal Expansion Coefficient	$\alpha_{PCM} = 3.18861 \cdot 10^{-4}$	$\left(\frac{1}{K}\right)$
Specific Heat	$c_{p,PCM} = 1626$	$\left(\frac{J}{kg \cdot K}\right)$
Conductivity	$k_{PCM} = 0.4886$	$\left(\frac{W}{m \cdot K}\right)$
Dynamic Viscosity	$\mu_{PCM} = 0.007008$	$\left(\frac{kg}{m \cdot s}\right)$
Solidus Temperature	$T_{sol} = 493.03$	(K)
Liquidus Temperature	$T_{liq} = 517.29$	(K)
Latent Heat	$\Lambda = 1.10 \cdot 10^5$	$\left(\frac{J}{kg}\right)$

(see fig. 3). The complete melting of the PCM lasts about $5h$. The melted PCM starts to melt near the heated internal wall and, due to the buoyancy force, it goes up filling the top part of the PCM enclosure where the liquid PCM goes from the inner wall toward the external wall of the PCM shell. A small portion of the melted front appears curvilinear in the top part and it moves from the top to the bottom during the process. On the other hand, below the top melted zone the vertical part of the melted front increases slowly its thick moving from the left to the right. The results remark the behaviour observed in previous literature in similar cases.

The external heating case (case 2) is represented in fig. 4, where only a 2D axisymmetric slice has been considered with the axis of the cylinder on the right hand side of the images and the external heated wall is on the left. Indeed, in this case the PCM starts to melt along the external heated wall. Therefore, the buoyancy force pushes the melted PCM on the top part of the PCM enclosure as described in the internal heating case. However, the melted PCM moves up along the external wall and in the top region pushes the liquid PCM toward the cylinder center. The flow direction has a positive influence on the convective motion due to the velocity increase of the melted PCM when it moves radially from the external wall to the center, due to continuity. Here, the whole melting front appears to have an higher velocity with respect to case 1 already in the early stage of the process. It moves from the left to the right during the melting process. Thus, the convective heat transfer in case of external heating appears enhanced with respect to case 1.

In fig. 5, the comparison of the space averaged liquid fraction with respect to the time gives the quantitative description of the phenomenon. The external heating shows a linear increasing of liquid fraction during the whole

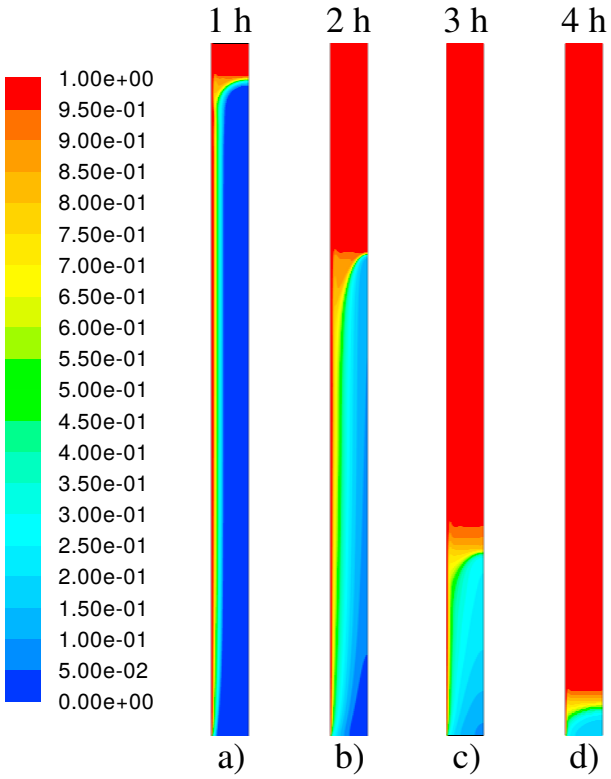

Fig. 3. Contours of the liquid fraction for the internal heating case (case 1). The internal heated wall is on the left hand side of the numerical domain, on the right hand side the external insulated wall is located.

process. On the other hand, the internal heating (case 1) shows a non linear increasing of the liquid fraction at the beginning and at the end of the process. The complete melting corresponds to about $5h$ and $2.5h$ for the internal heating (case 1) and external heating (case 2), respectively.

4. Conclusions

In the present work the influence of geometrical characteristics of the PCM enclosure has been investigated in two particular configurations. In detail, the first case consists in a well-known "shell-and-tube" configuration, where the heating of the PCM occurs from the internal duct toward the external PCM enclosure. The second configuration corresponds to an external heating of the PCM that is enclosed in a cylindrical vessel. Maintaining constant the volume of the PCM and the heating surface area, a comparison of the time to complete melting in both cases has been made. The results confirms, that even under equal boundary conditions the complete melting time is reduced of 50% considering an external heating with respect the internal one. It is worth noting that the convective heat transfer is heavily influenced by the geometrical characteristic of the LHTES device even without the increasing of area to volume ratio. The external heating of cylindrical tank filled with PCM appears to be a promising approach that worth to be investigated considering the influence of aspect ratio to increase even more their efficiency with respect to the classic shell-and tube configuration. The proposed external heating configuration can be used to develop simpler heat storage modules with respect to the shell-and-tube where a cross flow configuration with respect to the HTF can be used, as proposed in a schematic of a suitable application (see fig. 2). The present study could represent a starting point in the developing of new devices able to improve the heat transfer in LHTES applications.

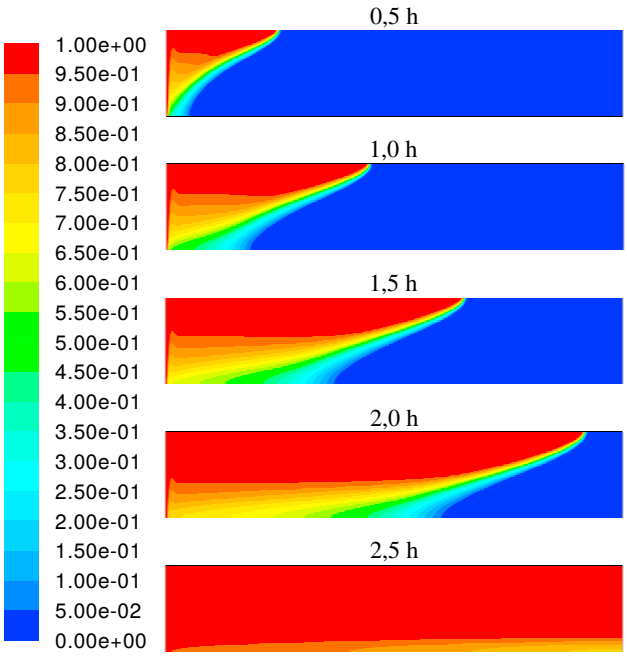

Fig. 4. Contours of the liquid fraction for the external heating case (case 2). The external heated wall is on the left hand side of the numerical domain, on the right hand side there is the axis of the cylinder.

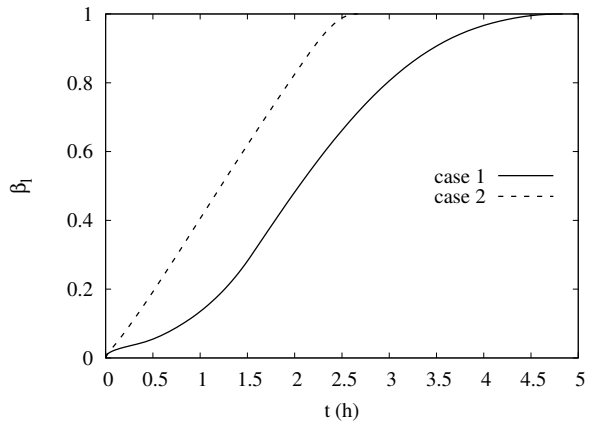

Fig. 5. Space averaged liquid fraction (β_l) within the PCM device with respect to the time (t) during the melting phase for internal heating (case 1) and external heating (case 2).

References

[1] Agyenim, F., Hewitt, N., Eames, P., Smyth, M., 2010. A review of materials, heat transfer and phase change problem formulation for latent heat thermal energy storage systems ('lhtess'). Renewable and Sustainable Energy Reviews 14, 615–628. doi:10.1016/j.rser.2009.10.015.

[2] Bennon, W., Incropera, F., 1987. A continuum model for momentum, heat and species transport in binary solid-liquid phase change systems-i. model formulation. International Journal of Heat and Mass Transfer 30, 2161–2170. doi:10.1016/0017-9310(87)90094-9.

[3] Bertrand, O., Binet, B., Combeau, H., Couturier, S., Delannoy, Y., Gobin, D., Lacroix, M., Le Qur, P., Mdale, M., Mencinger, J., Sadat, H., Vieira, G., 1999. Melting driven by natural convection a comparison exercise: First result. International Journal of Thermal Sciences 38, 5–26.

[4] Brent, A., Voller, V., Reid, K., 1988. Enthalpy-porosity technique for modeling convection-diffusion phase change: Application to the melting of a pure metal. Numerical Heat Transfer 13, 297–318. doi:10.1080/10407788808913615.

[5] Bufi, E., Camporeale, S., Fornarelli, F., Fortunato, B., Pantaleo, A., Sorrentino, A., Torresi, M., 2017. Parametric multi-objective optimization

of an organic rankine cycle with thermal energy storage for distributed generation. Energy Procedia 126, 429–436. doi:10.1016/j.egypro.2017.08.239.

[6] Fornarelli, F., Camporeale, S., Fortunato, B., Torresi, M., Oresta, P., Magliocchetti, L., Miliozzi, A., Santo, G., 2016a. Cfd analysis of melting process in a shell-and-tube latent heat storage for concentrated solar power plants. Applied Energy 164, 711–722. doi:10.1016/j.apenergy.2015.11.106.

[7] Fornarelli, F., Ceglie, V., Fortunato, B., Camporeale, S., Torresi, M., Oresta, P., Miliozzi, A., 2017. Numerical simulation of a complete charging-discharging phase of a shell and tube thermal energy storage with phase change material. Energy Procedia 126, 501–508. doi:10.1016/j.egypro.2017.08.220.

[8] Fornarelli, F., Lippolis, A., Oresta, P., 2016b. Buoyancy effect on the flow pattern and the thermal performance of an array of circular cylinders. Journal of Heat Transfer 139. doi:10.1115/1.4034794.

[9] Fornarelli, F., Oresta, P., Lippolis, A., 2015. Flow patterns and heat transfer around six in-line circular cylinders at low reynolds number. JP Journal of Heat and Mass Transfer 11, 1–28. doi:10.17654/JP2015_001_028.

[10] Gasia, J., Tay, N., Belusko, M., Cabeza, L., Bruno, F., 2017. Experimental investigation of the effect of dynamic melting in a cylindrical shell-and-tube heat exchanger using water as pcm. Applied Energy 185, 136–145. doi:10.1016/j.apenergy.2016.10.042.

[11] Gobin, D., Quéré, P., 2000. Melting from an isothermal vertical wall. synthesis of a numerical comparison exercise. Computer Assisted Mechanics and Engineering Sciences 7, 289–306.

[12] König-Haagen, A., Franquet, E., Pernot, E., Brggemann, D., 2017. A comprehensive benchmark of fixed-grid methods for the modeling of melting. International Journal of Thermal Sciences 118, 69–103. doi:10.1016/j.ijthermalsci.2017.04.008.

[13] Mehrabian, R., Keane, M., Flemings, M., 1970a. Experiments on macrosegregation and freckle formation. Metallurgical Transactions 1, 3238–3241. doi:10.1007/BF03038445.

[14] Mehrabian, R., Keane, M., Flemings, M., 1970b. Interdendritic fluid flow and macrosegregation; influence of gravity. Metallurgical and Materials Transactions 1, 1209–1220. doi:10.1007/BF02900233.

[15] Ming, Z., Li, S., Yanying, H., 2015. Status, challenges and countermeasures of demand-side management development in china. Renewable and Sustainable Energy Reviews 47, 284–294. doi:10.1016/j.rser.2015.03.028.

[16] Minkowycz, W., 1996. Advances In Numerical Heat Transfer. volume 1 of *Advances in numerical heat transfer*. Taylor & Francis.

[17] Pielichowska, K., Pielichowski, K., 2014. Phase change materials for thermal energy storage. Progress in Materials Science 65, 67–123. doi:10.1016/j.pmatsci.2014.03.005.

[18] Söder, L., Lund, P., Koduvere, H., Bolkesjø, T., Rossebø, G., Rosenlund-Soysal, E., Skytte, K., Katz, J., Blumberga, D., 2018. A review of demand side flexibility potential in northern europe. Renewable and Sustainable Energy Reviews 91, 654–664. doi:10.1016/j.rser.2018.03.104.

[19] Voller, V., Cross, M., Markatos, N., 1987. An enthalpy method for convection/diffusion phase change. International Journal for Numerical Methods in Engineering 24, 271–284. doi:10.1002/nme.1620240119.

[20] Voller, V., Prakash, C., 1987. A fixed grid numerical modelling methodology for convection-diffusion mushy region phase-change problems. International Journal of Heat and Mass Transfer 30, 1709–1719. doi:10.1016/0017-9310(87)90317-6.

[21] Šarler, B., Kuhn, G., 1998a. Dual reciprocity boundary element method for convective-diffusive solid-liquid phase change problems, part 1. formulation. Engineering Analysis with Boundary Elements 21, 53–62.

[22] Šarler, B., Kuhn, G., 1998b. Dual reciprocity boundary element method for convective-diffusive solid-liquid phase change problems, part 2. numerical examples. Engineering Analysis with Boundary Elements 21, 65–79.